Inhomogeneous magnetism in La-doped $CaMnO_3$. II. Nanometric-scale spin clusters and long-range spin canting

E. Granado,[1,2,3,*] C. D. Ling,[4,5] J. J. Neumeier,[6] J. W. Lynn,[1,2] and D. N. Argyriou[5]
[1]*NIST Center for Neutron Research, National Institute of Standards and Technology, Gaithersburg, Maryland 20899, USA*
[2]*Center for Superconductivity Research, University of Maryland, College Park, Maryland 20742, USA*
[3]*Laboratório Nacional de Luz Síncrotron, Caixa Postal 6192, CEP 13084-971, Campinas, SP, Brazil*
[4]*Institut Laue-Langevin, BP 156, 38042 Grenoble Cedex 9, France*
[5]*Materials Science Division, Argonne National Laboratory, Argonne, Illinois 60439, USA*
[6]*Department of Physics, Montana State University, Bozeman, Montana 59717, USA*
(Received 14 March 2003; published 23 October 2003)

Neutron measurements on $Ca_{1-x}La_xMnO_3$ ($0.00 \leqslant x \leqslant 0.20$) reveal the development of magnetic droplets showing a liquidlike intercluster spatial distribution. The average size of the droplets is ~ 10 Å, the concentration of which in the *G*-AFM matrix being proportional to x (one cluster per ~ 60 doped electrons). In addition, a long-range ordered ferromagnetic component is observed for $0.05 \lesssim x \lesssim 0.14$. This component is perpendicularly coupled to the simple *G*-type antiferromagnetic (*G*-AFM) structure of the undoped compound, which is a signature of a *G*-AFM+FM spin-canted state. The possible relationship between cluster formation and the stabilization of a long-range spin canting for intermediate doping is discussed.

DOI: 10.1103/PhysRevB.68.134440 PACS number(s): 75.25.+z, 61.12.−q, 61.25.−f, 75.60.−d

I. INTRODUCTION

Doped manganites are strongly correlated electron systems with unusually large responses to external perturbations such as magnetic field and pressure. While the most dramatic effects such as colossal magnetoresistance have been observed in heavily doped compounds, systematic studies on lightly and moderately doped samples may reveal some fundamental aspects of manganite physics. In these regimes, the antiferromagnetic (AFM) spin structures shown by the undoped compounds[1] tend to be destabilized by the ferromagnetic (FM) exchange interactions mediated through the charge carriers. For electron-doped $CaMnO_3$, a relatively weak ferromagnetism has been observed up to $\sim 15\%$ doping.[2–6] While the classic de Gennes theory for lightly doped manganites describes the weak ferromagnetism in terms of spin-canted ground states,[7] a number of more recent theoretical studies indicates that homogeneous canted magnetic structures may not be energetically stable, suggesting a tendency towards magnetic and electronic phase segregation for both hole-doped[8–17] and electron-doped[14–18] manganites. In fact, for moderately hole-doped $LaMnO_3$ (5–8 % Ca or Sr doping), single crystal neutron-scattering studies revealed the existence of nanometric-scale magnetic inhomogeneities at low T.[19–21] Whether electron-doped manganites actually mirror this effect is an open experimental problem and a fundamental issue, since the phase diagram of electron-doped manganites is in general asymmetrical with respect to their hole-doped counterparts. For instance, the ferromagnetic metallic ground state is not realized for La-doped $CaMnO_3$, in stark contrast with the wide compositional interval where this state is observed in Ca-doped $LaMnO_3$.

Previous dc-magnetization,[5,22] thermal conductivity,[22] Raman-scattering,[23] and electron spin resonance[23] studies on $Ca_{1-x}La_xMnO_3$ indicate a crossover between distinct doping regimes at $x \sim 0.03$, which in this paper we refer to as low-doping ($0 < x \lesssim 0.03$) and intermediate-doping ($0.03 \lesssim x \lesssim 0.15$) regimes. While it has been suggested that this crossover may reflect novel polaron physics,[22] not much direct information on the microscopic structure of the weak ferromagnetism observed for electron-doped manganites is presently available. A notable exception is a NMR study performed on $Ca_{1-x}Pr_xMnO_3$ ($x \leqslant 0.1$),[24] which found a coexistence of ferromagnetism and antiferromagnetism in the samples studied, thus supporting a phase segregation scenario.

This paper is the second part of an extensive study of the magnetic and crystallographic ground states of La-doped $CaMnO_3$. Part I described the general relationships among the ground states revealed by an investigation of the mesoscopic-scale phase separation inherent to this system.[25] It is relevant to note that the results described in Part I indicate that the FM moments are developed within *G*-AFM mesoscopic domains.[25] This is deduced from the coincidence of the FM and *G*-AFM ordering temperatures and from the concomitant decrease of the *G*-AFM and FM moments, on the one hand, and the increase of the *C*-AFM moment, on the other hand, as the doping level increases.[25] Schematic representations of the *G*-AFM and *C*-AFM structures are given in Fig. 1 of Part I. In Part II we focus on the microscopic nature of the weak ferromagnetic moment observed in the *G*-AFM matrix for $0.00 < x \lesssim 0.15$. The most detailed investigations are performed on the compounds with $x = 0.02$ and 0.09, which are representative members of the low- and intermediate-doping regimes, respectively. Elastic neutron scattering at low angles reveals a liquidlike spatial distribution of magnetic clusters of average size ~ 10 Å in both regimes, whose concentration is proportional to the doping level. Neutron-diffraction measurements under applied magnetic fields reveal that the *G*-AFM and FM spin components

are uncoupled for low doping and become orthogonally coupled as the doping increases. Such an orthogonal coupling is a signature of a spin-canted state. Small-angle neutron scattering (SANS) measurements also show magnetic domain-wall scattering in the intermediate doping regime, revealing a long-range FM component. The combined results severely limit the possible scenarios for the development of the FM moment in electron-doped manganites. In fact, they indicate a nontrivial microscopic magnetism for this system, which cannot be described either by a homogeneously spin-canted state,[7] or by a radical phase segregation where FM clusters are embedded into a pure *G*-AFM matrix. The phase diagram of La-doped $CaMnO_3$, revealed by the combination of the results described in Parts I and II, is given in Fig. 6(b) of Part I.[25]

II. EXPERIMENTAL DETAILS

Ceramic pellets of $Ca_{1-x}La_xMnO_3$ ($x=0.00$, 0.02, 0.03, 0.05, 0.06, 0.07, 0.09, 0.12, 0.16, and 0.20) were prepared by standard solid state reaction, as described in detail in the previous paper.[25] A hole-doped sample, $Ca_{0.05}La_{0.95}MnO_3$, was prepared in a similar manner to the other samples, but was reacted in Argon at all stages of the preparation and reacted to a maximum temperature of 1250 °C to keep the defect concentration low.

Elastic neutron scattering experiments at low angles were performed using the BT-2 triple-axis spectrometer at the NIST Center for Neutron Research, with $E=14.7$ meV and $(60'-20'-20'-open)$ collimation. Magnetic-field-dependent neutron powder diffraction experiments were performed on the same spectrometer with $E=14.7$ meV and $(60'-40'-40'-open)$ collimation. The field was applied perpendicularly to the plane defined by the incident and scattered wave vectors, using a superconducting magnet.

The SANS experiments were carried out using the NG-1 instrument at NIST, with $\lambda=12$ Å, and a sample-detector distance of 3.5 m. The intensities were measured by a two-dimensional position-sensitive detector ($0.007\ Å^{-1}<Q<0.08\ Å^{-1}$), and were angularly averaged around the beam-center position.

III. RESULTS AND ANALYSIS

A. Low-doping regime

The inset of Fig. 1(a) shows the elastic neutron scattering at 10 and 200 K for $Ca_{0.98}La_{0.02}MnO_3$, in the Q interval between 0.05 and 0.7 $Å^{-1}$. The elastic magnetic scattering at low-T [$I_M(Q)$] can be more readily identified by subtracting the elastic scattering of the paramagnetic phase at 200 K from the intensities of the magnetically ordered phase at 10 K. This is shown in Fig. 1(a) (symbols). The solid lines are fits to a model of rigid magnetic droplets showing a liquid-like intercluster spatial distribution.[20,21,26] The full expression for $I_M(Q)$ under this model is given in Ref. 20. The shape of $I_M(Q)$ is determined by the minimum distance between clusters (d_{min}), the droplet diameter (D), and the cluster concentration (N_V). For $x=0.02$, the fitting parameters are $d_{min}=41(3)$ Å, $N_V=6.6(1.4)\times10^{-6}\ Å^{-3}$ [i.e., one droplet per $\sim59(12)$ doping electrons], and $D=10.4(1.8)$ Å (see Ref. 27). Errors given in parentheses are statistical only and represent one standard deviation. Fits to $I_M(Q)$ of Fig. 1 assuming clusters with soft walls were also performed, providing equally good fits to the experimental data and nearly identical results for N_V and d_{min}. In fact, the calculated profiles are mostly determined by inter-cluster diffraction, except for the overall intensity decay at $Q\gtrsim0.4\ Å^{-1}$ due to the finite cluster size. Thus, little information on the cluster shape and rigidity can be directly obtained from this experiment.

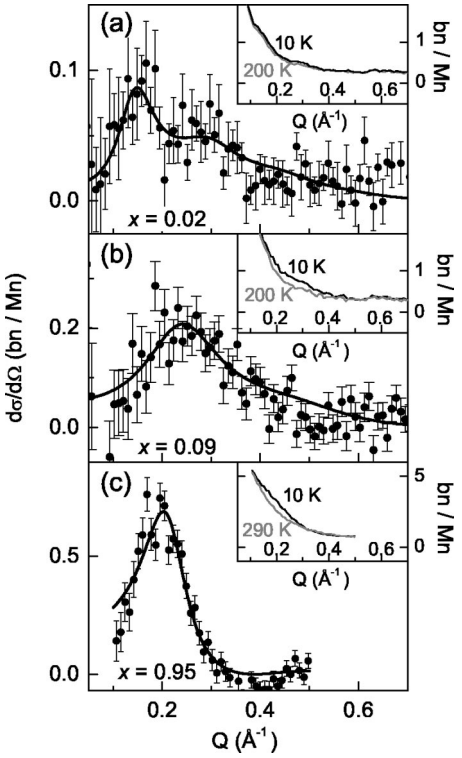

FIG. 1. Elastic magnetic cross section versus Q for $Ca_{1-x}La_xMnO_3$ for $x=0.02$ (a), $x=0.09$ (b), and $x=0.95$ (c). The solid lines are fits to a liquid-like distribution model of magnetic droplets (see the text). The insets show the raw data at 10 and 200 K (290 K for $x=0.95$).

In order to demonstrate the reproducibility of the above method for experiments taken at different conditions, and check the sensitivity of the results to sample preparation methods, elastic scattering experiments were also performed at 10 and 290 K on a polycrystalline hole-doped manganite, $Ca_{0.05}La_{0.95}MnO_3$ [see Fig. 1(c)]. The subtracted intensity, $I(10\ K)-I(290\ K)$, shows a peak at $Q\sim0.2\ Å^{-1}$, for which the intensity, shape and width are in good agreement with previously published results for a single crystal of the same compound.[21] This indicates that the magnetic clusters observed for lightly hole-doped manganites[20,21] are essentially insensitive to the sample growth method. This result, combined with the evidence of magnetic clusters reported here for electron-doped manganites, supports a universal tendency for inhomogeneous ground states in lightly doped manganites.

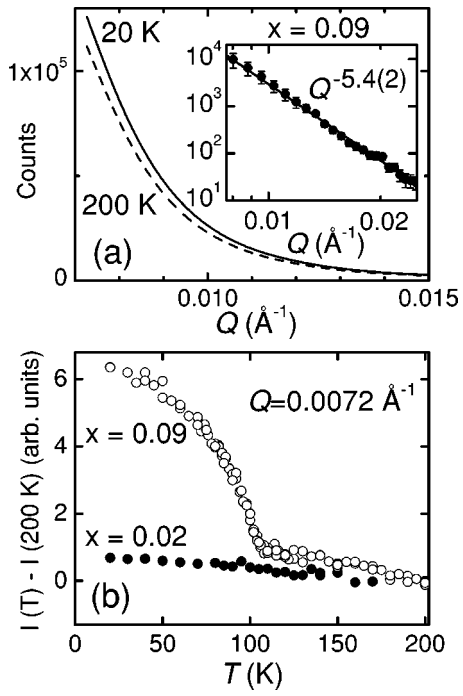

FIG. 2. (a) SANS for $Ca_{1-x}La_xMnO_3$ at 20 and 200 K for $x=0.09$. The inset shows $I(20\ \mathrm{K})-I(200\ \mathrm{K})$ and a fit to a power law. (b) T dependence of the scattering at $Q=0.0072\ \mathrm{\AA}^{-1}$ for $x=0.02$ and 0.09. Data in (b) were corrected for thickness and absorption to allow a direct comparison between samples.

The possibility of a long-range FM component was investigated by energy-integrated SANS. The FM scattering peaks at $Q=0$, and shows a distribution in the Q scale of $\sim 2\pi/L_d$, where L_d is the average domain size. The SANS data on electron-doped manganites are dominated by a nonmagnetic and slightly T-dependent component (most likely from intergrain scattering). For $x \lesssim 0.03$, no evidence for domain-wall scattering was observed by SANS, within our experimental sensitivity [see Fig. 2(b), filled circles].

To clarify the microscopic relationship between the FM signal and the G-AFM spin component, H-dependent neutron diffraction experiments were carried out. The magnetic intensities are proportional to the square of the sublattice magnetization, and also to the geometrical factor $\gamma \equiv \langle 1-(\hat{\mathbf{M}}\cdot\hat{\boldsymbol{\tau}})^2\rangle$, where $\hat{\boldsymbol{\tau}}$ and $\hat{\mathbf{M}}$ are the directions of the reciprocal lattice vector and the sublattice magnetization, respectively, and the brackets account for a domain average. For cubic or quasicubic crystal lattices, $\gamma(\mathbf{H}=0)=2/3$. Under the application of $\mathbf{H}$, the FM component reorients along the field direction. Therefore, for increasing $\mathbf{H}\perp\hat{\boldsymbol{\tau}}$, such as in our experiment, one has $\gamma_{FM}(\mathbf{H})\rightarrow 1$. The coupling of the AFM moments to the FM moments can be inferred from the $\mathbf{H}$ dependence of γ_{AFM} (also see Refs. 1 and 28).

For $x=0.02$, the field-induced reorientation of the FM spin component could not be probed by H-dependent neutron diffraction, due to the very small moments. To this end, dc-magnetization (M_{dc}) measurements were taken using a commercial superconducting quantum interference device magnetometer. The inset of Fig. 3(a) shows the H dependence of M_{dc} at 5 K. The curve can be decomposed into a FM signal

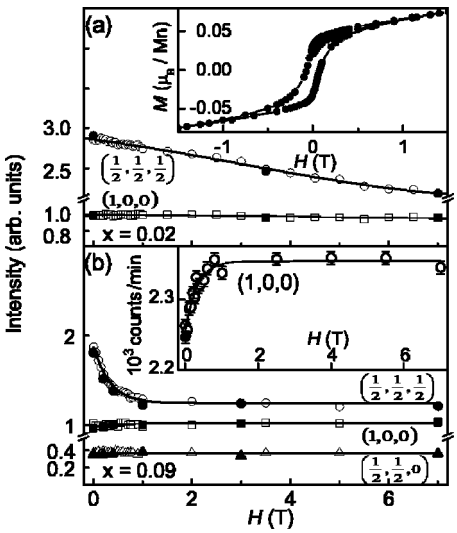

FIG. 3. H dependence at 5 K of the intensity of the $(\frac{1}{2},\frac{1}{2},\frac{1}{2})$ G-AFM and (1,0,0) nuclear + FM Bragg reflections for $x=0.02$ (a) and $x=0.09$ (b), and $(\frac{1}{2},\frac{1}{2},0)$ C-AFM reflection for $x=0.09$ (cubic notation). Empty (filled) symbols represent increasing (decreasing) fields. The insets show the H dependence at 5 K of the dc magnetization for $x=0.02$ and of the peak intensity of the (1,0,0) Bragg reflection for $x=0.09$.

which saturates at $\sim 0.05\mu_B$/Mn for fields smaller than 0.5 T, and a linear component which is tentatively ascribed to a conventional field-induced spin canting. The field-dependence of the G-AFM spins for $x=0.02$ was probed by neutron diffraction [see Fig. 3(a)]. An intensity decrease of the $(\frac{1}{2},\frac{1}{2},\frac{1}{2})$ reflection was observed in the field scale of several tesla. This effect is not directly connected to the reorientation of the spontaneous FM moments, which takes place for $H<0.5$ T [see the inset of Fig. 3(a)]. Thus, for $x=0.02$, the G-AFM moments are not directly coupled to the FM moments, at least for small fields ($H<0.5$ T). We note that the FM and AFM components must be perpendicularly coupled in a spin-canted state. Thus, the absence of such a coupling at the low-doping regime demonstrates that the origin of the weak FM signal is not due to a zero-field spin canting of the G-AFM structure. Although this conclusion might, at first sight, have been anticipated by the presence of magnetic clusters shown in Fig. 1(a), in Sec. III B we show that the presence of nanometric magnetic clusters does not exclude the possibility of a spin-canted state. In fact, signatures of both nanometric clusters and long-range spin canting have been found at the intermediate-doping regime (see below).

B. Intermediate-doping regime

The inset of Fig. 1(b) shows the elastic neutron scattering at 10 and 200 K for $Ca_{0.91}La_{0.09}MnO_3$, in the Q interval between 0.05 and 0.7 $\mathrm{\AA}^{-1}$. The elastic magnetic scattering at low-T [$I_M(Q)$] is shown in Fig. 1(b) (symbols). The solid lines are fits to the same model used to fit the data at the low-doping regime (see above). For $x=0.09$, we obtain $d_{min}=24(2)$ Å, $N_V=28(6)\times 10^{-6}$ $\mathrm{\AA}^{-3}$ [one cluster per 63(14) doping electrons], and $D=10.6(1.6)$ Å (see Ref. 27).

Figure 2(a) shows energy-integrated SANS at 10 and 200 K for $x=0.09$. Besides the slightly T-dependent intergrain scattering, a magnetic component is also clearly present for $x \geqslant 0.05$. This is evidenced by the T dependence of the scattering at $Q=0.0072$ Å^{-1}, showing a significant enhancement below T_C [$=108(1)$ K for $x=0.09$; see Fig. 2(b)]. The inset of Fig. 2(a) shows the intensities at 10 K after subtracting the background scattering at 200 K, and a fit to a power-law behavior, $I=AQ^{-5.4(2)}$, for Q between 0.007 and 0.025 Å^{-1}. This result indicates the existence of magnetic domains with sizes of several hundred angstroms or larger, evidencing a long-range FM component. This conclusion is also supported by polarization-dependent neutron diffraction of a nuclear Bragg peak for $x=0.09$, which showed the neutron beam being depolarized by the sample below T_C (not shown).

As explored in detail in the previous paper,[25] the compounds belonging to the intermediate doping regime show crystallographic and magnetic mesoscopic phase separations at low-T; magnetic Bragg peaks associated with C-AFM, G-AFM, and FM orders have been observed.[25] Figure 3(b) shows the field dependence of the (1,0,0) nuclear + FM, $(\frac{1}{2},\frac{1}{2},\frac{1}{2})$ G-AFM, and $(\frac{1}{2},\frac{1}{2},0)$ C-AFM Bragg peaks (cubic notation) for $Ca_{0.91}La_{0.09}MnO_3$. The inset of Fig. 3(b) shows the peak intensity of the (1,0,0) reflection in detail. The observed increase of this peak intensity for increasing fields up to ~ 0.5 T indicates a reorientation of the FM spin component along the field direction (see Sec. III A). The intensity of the $(\frac{1}{2},\frac{1}{2},\frac{1}{2})$ peak decreases by 34(3)% in the same field range, indicating a perpendicular coupling between G-AFM and FM spin components, consistent with G-AFM + FM spin canting. The intensity of the $(\frac{1}{2},\frac{1}{2},0)$ peak is insensitive to fields up to 7 T, showing that the C-AFM spin component is not coupled to the FM spin component. Thus, the results shown in Fig. 3(b), combined with high-resolution diffraction data,[25] suggest a mesoscopic phase coexistence between C-AFM regions with no FM moment and regions with coupled G-AFM+FM moments for intermediate dopings.

Thus, nanometric-scale magnetic clusters have been observed for both low and intermediate La-doping regimes of $CaMnO_3$, the concentration of which is proportional to the doping level. Still, the nature of the ferromagnetic moments seem to be significantly different at both doping regimes. For intermediate doping, a long-range ferromagnetic moment has been evidenced by SANS measurements (see Fig. 2), and the G-AFM moment is orthogonally coupled to the FM component (see Fig. 3), suggesting a long-range ordered spin canting of the G-AFM phase. Such effects were not observed at the low-doping regime. The combined results suggest that La doping in $CaMnO_3$ leads to the formation of nanometric-scale FM clusters which are isolated for sufficiently low doping, while for intermediate doping a canting of the G-AFM spin matrix where the FM clusters are embedded takes place. The implications of this interesting scenario are more thoroughly discussed below.

IV. DISCUSSION

The observation of magnetic clusters (see Fig. 1) clearly points to a spatially inhomogeneous charge-carrier distribution in this system. The ratio between doped electrons and cluster densities (~ 60, see above) is independent of x for electron-doped manganites and is identical to that found in hole-doped manganites,[20,21] strongly suggesting a universal behavior. However, this large ratio and the small dimensions of the observed clusters (comprising ~ 10 unit cells) make it clear that only a fraction of the doped electrons are inside such clusters. The correct mechanism that leads to this phenomenon is not clear at this point. Even with a few electrons in each cluster, the charge contrast inside and outside the droplets may be exceedingly high, particularly in the low-doping regime. Simple electrostatic considerations indicate that the Coulomb energy loss for a FM two-electron droplet with $D \sim 10$ Å surrounding a La^{3+} ion is of the order of 1 eV for low- and intermediate-doping regimes, and increases quadratically with the number of cluster electrons. This Coulomb energy might overwhelm the delocalization energy gain per electron in the cluster ($t \sim 0.1-1$ eV), as already pointed out by Chen and Allen.[29] In this context, it would appear natural to consider that clusters might be formed by electrostatic attraction in La-rich regions of the sample, presumably associated with intrinsic chemical inhomogeneities.[30] This mechanism would lead to electrically-neutral, Mn^{3+}-rich, magnetic clusters. The relatively small cluster densities would be naturally accounted for in this scenario. On the other hand, the cluster diffraction profiles shown in Figs. 1(a) and 1(b) imply a spatial short-range order similar to a liquid state, as opposed to a cluster gas where the cluster positions would be uncorrelated. Such an order suggests intercluster repulsion, presumably dictated by Coulomb forces between electrically charged and mobile clusters. The cluster diffraction also implies that neighboring clusters are magnetically correlated in both low- and intermediate-doping regimes, as opposed to a superparamagnetic state. In view of the above considerations, we believe that a truly intrinsic mechanism for small cluster formation in this system, i.e., not caused by chemical inhomogeneities, might not be discarded at this point.

The electrons outside the small magnetic clusters discussed above are likely to be important for the overall magnetic behavior of La-doped $CaMnO_3$. In fact, using the fitting parameters obtained from Fig. 1, the total cluster contributions to the sample-average magnetizations are estimated to be $0.02(1)\mu_B$/Mn for $x=0.02$ and $0.04(2)\mu_B$/Mn for $x=0.09$, which are significantly smaller than the saturation magnetizations obtained from dc magnetometry, $0.05\mu_B$/Mn and $0.40\mu_B$/Mn, respectively.[5] Also, the combination of a long-range FM spin component and the orthogonal coupling between FM and G-AFM spin components at intermediate doping is a signature of a long-range G-AFM+FM spin-canted state that does not appear to be accomplished at the low-doping regime. Although the present set of experimental data, combined with previous work on La-doped $CaMnO_3$,[4,5,22,23] may be insufficient to lead to a complete description for the microscopic structure of the FM moments and doped electrons in this system, it severely constrains any plausible model, as described below.

It is clear from the results above that a second type of doped electron is present in La-doped $CaMnO_3$, besides the

type forming relatively small FM clusters ($D \sim 10$ Å). Given the long-range spin-canted state evidenced for intermediate doping, the extra electrons seem to be delocalized on the atomic scale. On the other hand, the fact that a metallic state is not accomplished at low temperatures,[4] combined with the absence of an observable long-range FM component at low doping, suggests that such extra electrons are not fully delocalized into a de Gennes canted state[7] either. Thus, we suggest that these electrons are segregated into spin-canted regions of finite size, presumably larger than the small FM clusters directly observed by neutrons. These regions would overlap for intermediate-doping, leading to the observed long-range FM component perpendicularly coupled to the *G*-AFM moments. We note that such hypothetical spin-canted clusters were not directly observed in our neutron scattering measurements, possibly due to the small magnetization contrast and/or large sizes leading to small differential cross section in the *Q* region accessible for elastic measurements (see Fig. 1). From a theoretical point of view, the formation of an inhomogeneous *G*-AFM+FM spin-canted state in electron-doped manganites, evidenced in this work, might be the result of a balance between the well-known electronic instability of the homogeneous spin-canted *G*-AFM state[14–18] and the large Coulomb energy cost of a radical phase segregation scenario where purely FM droplets are formed into a pure *G*-AFM background.

V. CONCLUSIONS

Our results on La-doped $CaMnO_3$ indicate that a fraction of the doped electrons segregate into small ($D \sim 10$ Å) FM clusters embedded in the *G*-AFM matrix of the undoped compound. The remaining electrons are presumably delocalized over a more extended volume, leading to an inhomogeneous spin-canted state at intermediate doping. The density of the 10-Å clusters, as well as the FM component of the spin-canted state, increase with the doping level, and the overall FM moment becomes increasingly dominant over the *G*-AFM spin component. Nevertheless, the pure FM metallic state is never stabilized for La-doped $CaMnO_3$, due to the gradual emergence of the orbitally polarized *C*-AFM state for $x \gtrsim 0.06$, which competes with the *G*-AFM + FM state through a first-order phase transition, as explored in the previous paper.[25] This competition leads to mesoscopic magnetic and crystallographic phase separation over large *x* and *T* intervals, and finally to the stabilization of the *C*-AFM phase for $0.16 \lesssim x \lesssim 0.20$.[25,31–33]

ACKNOWLEDGMENTS

This work was supported by FAPESP, Brazil, NSF-MRSEC, DMR 0080008, NSF DMR 9982834, and U.S. Department of Energy, Basic Energy Sciences - Materials Sciences, Contract No. W-31-109-ENG-38, USA.

*Email address: granado@lnls.br

[1] E.O. Wollan and W.C. Koehler, Phys. Rev. **100**, 545 (1955).
[2] H. Chiba, M. Kikuchi, K. Kusaba, Y. Muraoka, and Y. Syono, Solid State Commun. **99**, 499 (1996).
[3] A. Maignan, C. Martin, F. Damay, and B. Raveau, Chem. Mater. **10**, 950 (1998).
[4] J.J. Neumeier and D.H. Goodwin, J. Appl. Phys. **85**, 5591 (1999).
[5] J.J. Neumeier and J.L. Cohn, Phys. Rev. B **61**, 14 319 (2000).
[6] H. Aliaga, M.T. Causa, B. Alascio, H. Salva, M. Tovar, D. Vega, G. Polla, G. Leyva, and P. Konig, J. Magn. Magn. Mater. **226-230**, 791 (2001).
[7] P.-G. de Gennes, Phys. Rev. **118**, 141 (1960).
[8] L.-J. Zou, Q.-Q. Zheng, and H.Q. Lin, Phys. Rev. B **56**, 13 669 (1997).
[9] S. Yunoki, J. Hu, A.L. Malvezzi, A. Moreo, N. Furukawa, and E. Dagotto, Phys. Rev. Lett. **80**, 845 (1998).
[10] D.P. Arovas and F. Guinea, Phys. Rev. B **58**, 9150 (1998).
[11] M. Yamanaka, W. Koshibae, and S. Maekawa, Phys. Rev. Lett. **81**, 5604 (1998).
[12] E.L. Nagaev, Phys. Rev. B **58**, 2415 (1998).
[13] M.Yu. Kagan, D.I. Khomskii, and M.V. Mostovoy, Eur. Phys. J. B **12**, 217 (1999).
[14] S. Yunoki and A. Moreo, Phys. Rev. B **58**, 6403 (1998).
[15] E. Dagotto, S. Yunoki, A.L. Malvezzi, A. Moreo, J. Hu, S. Capponi, D. Poilblanc, and N. Furukawa, Phys. Rev. B **58**, 6414 (1998).
[16] S.-Q. Shen and Z.D. Wang, Phys. Rev. B **58**, R8877 (1998).
[17] H. Yi and J. Yu, Phys. Rev. B **58**, 11 123 (1998).
[18] S.M. Dunaevsky and V.V. Deriglazov, Phys. Rev. B **67**, 014409 (2003).
[19] M. Hennion, F. Moussa, J. Rodríguez-Carvajal, L. Pinsard, and A. Revcolevschi, Phys. Rev. B **56**, R497 (1997).
[20] M. Hennion, F. Moussa, G. Biotteau, J. Rodríguez-Carvajal, L. Pinsard, and A. Revcolevschi, Phys. Rev. Lett. **81**, 1957 (1998).
[21] M. Hennion, F. Moussa, G. Biotteau, J. Rodríguez-Carvajal, L. Pinsard, and A. Revcolevschi, Phys. Rev. B **61**, 9513 (2000).
[22] J.L. Cohn and J.J. Neumeier, Phys. Rev. B **66**, 100404(R) (2002).
[23] E. Granado, N.O. Moreno, H. Martinho, A. García, J.A. Sanjurjo, I. Torriani, C. Rettori, J.J. Neumeier, and S.B. Oseroff, Phys. Rev. Lett. **86**, 5385 (2001).
[24] M.M. Savosta, P. Novák, M. Marysko, Z. Jirák, J. Hejtmánek, J. Englich, J. Kohout, C. Martin, and B. Raveau, Phys. Rev. B **62**, 9532 (2000).
[25] C.D. Ling, E. Granado, J.J. Neumeier, J.W. Lynn, and D.N. Argyriou, preceding paper, Phys. Rev. B **68**, 134439 (2003).
[26] N.W. Ashcroft and J. Lekner, Phys. Rev. **145**, 83 (1966).
[27] An estimation of the difference between the average magnetization inside and outside the droplets (δM) may be obtained from the cross sections, as described in Ref. 20. We obtain $\delta M = 6(3)\ \mu_B$/Mn for $x = 0.02$ and 0.09. The large standard deviation is mostly due to the uncertainty in the cluster volume. For $x = 0.09$, we considered that the droplets are distributed in the $\sim 50\%$ volume fraction occupied by the G-AFM + FM mesoscopic domains (see the text and Ref. 26). Thus, the actual differential cross sections for droplet scattering from such mesoscopic domains is twice the sample-average cross sections shown in Fig. 1(b). The fitting parameter N_V refers, by definition, to the cluster concentration inside the mesoscopic domains where the clusters are located.
[28] E. Granado, H. Martinho, M.S. Sercheli, P.G. Pagliuso, D.D. Jackson, M. Torelli, J.W. Lynn, C. Rettori, Z. Fisk, and S.B. Oseroff, Phys. Rev. Lett. **89**, 107204 (2002).

[29] Y.-R. Chen and P.B. Allen, Phys. Rev. B **64**, 064401 (2001).
[30] T. Shibata, B. Bunker, J.F. Mitchell, and P. Schiffer, Phys. Rev. Lett. **88**, 207205 (2002).
[31] P.N. Santhosh, J. Goldberger, P.M. Woodward, T. Vogt, W.P. Lee, and A.J. Epstein, Phys. Rev. B **62**, 14 928 (2000).
[32] M. Pissas, G. Kallias, M. Hofmann, and D.M. Többens, Phys. Rev. B **65**, 064413 (2002).
[33] M. Pissas and G. Kallias, cond-mat/0205410 (unpublished).